A framework for estimating epistemic uncertainty in LES closures

By L. Jofre, S. P. Domino† AND G. Iaccarino

1. Motivation and objectives

Over the past decade, large-eddy simulation (LES) has gained significant importance as a high-fidelity reference technique for the numerical resolution of turbulent flow. One of the main reasons is the tremendous growth in available computational power, which has made its superior accuracy attractive with respect to other cost-effective methods like the Reynolds-averaged Navier-Stokes (RANS) equations. Moreover, despite the presumably further increase in computing resources through the deployment of upcoming exascale supercomputers — 1-10k times augmented floating-point capacity is foreseen (DoE 2012) —, the expectation in the computational community is that LES will continue its consolidation as a workhorse methodology for engineering applications and multiscale problems, whereas direct numerical simulation (DNS) will remain as the gold standard technique, affordable only in very expensive scientific studies. In comparison to DNS, LES approaches reduce the computational cost of solving turbulent flow by removing small-scale information from the governing equations via low-pass filtering. However, the effects of the small scales on the resolved flow field are not negligible, and therefore their contribution in the form of subfilter stresses needs to be modeled. As a consequence, the assumptions introduced in the closure formulations result in potential sources of structural uncertainty that can affect the quantities of interest (QoI). Hence, it is of remarkable utility the development of a framework capable to effectively estimate these effects on complex scenarios.

Even with the widespread utilization of LES in many scientific and technological areas, there have been few studies in which model-form incertitude has been analyzed from an uncertainty quantification (UQ) viewpoint. In general, most are based on non-intrusive methodologies applied to simple flow configurations, and are concerned mainly with sensitivities to LES closure parameters (Lucor *et al.* 2007), such as model coefficients (Meldi *et al.* 2011), filter characteristics (Meyers & Sagaut 2007*a*) or mesh resolution (Meyers & Sagaut 2007*b*). This type of analyses, although useful from the practitioner's perspective, present important impediments to generalization due to their dependency on the underlying structure of the models utilized. In order to overcome this limitation, this work aims to develop a framework for the estimation of structural uncertainty in LES closures that is independent of the initial model form. The strategy feeds from the methodology previously introduced in the context of RANS approaches (Gorlé & Iaccarino 2013; Emory *et al.* 2013), although there are important differences due to the inherent distinction between the two turbulence-resolution techniques. In short, the framework is based on introducing perturbations to the modeled turbulent stress tensor. These correspond to discrepancy in the magnitude (trace), shape (eigenvalues) and orientation (eigenvectors) of the normalized subfilter stresses with respect to a given tensor state.

† Sandia National Laboratories

In this research brief, the UQ framework is presented and a preliminary numerical investigation is performed. The report is organized as follows. In Section 2, the governing equations of LES are summarized. A detailed analysis of the filtered advection term is presented in Section 3. The methodology for epistemic incertitude estimation is described in Section 4. Exploratory numerical results for plane channel flow are reported in Section 5. Finally, conclusions are drawn and future work is outlined in Section 6.

2. Large-eddy simulation equations

The governing LES equations are derived by applying a low-pass filter, G, to the Navier-Stokes equations. The filter decomposes any flow variable $\phi(\mathbf{x}, t)$ into large-, $\overline{\phi}$, and small-scale, ϕ', contributions, i.e., $\phi = \overline{\phi} + \phi'$. The filtered part is defined as

$$\overline{\phi}(\mathbf{x}, t) = \int_\Omega G(\mathbf{x}, \mathbf{x}', \Delta)\phi(\mathbf{x}', t)\, d\mathbf{x}', \tag{2.1}$$

with $\mathbf{x}$ and $\mathbf{x}'$ position vectors in the domain Ω, and Δ the characteristic width of the filter.

Assuming that differentiation and filtering commute, the filtered incompressible Navier-Stokes equations result in

$$\frac{\partial \overline{u}_i}{\partial x_i} = 0, \tag{2.2}$$

$$\frac{\partial \overline{u}_i}{\partial t} + \frac{\partial (\overline{u_i u_j})}{\partial x_j} = -\frac{1}{\rho}\frac{\partial \overline{p}}{\partial x_i} + \nu \frac{\partial^2 \overline{u}_i}{\partial x_j \partial x_j}, \tag{2.3}$$

where u_i and p are the velocity vector and pressure variables, and ρ and ν are the density and kinematic viscosity of the fluid. This system is undetermined since it contains more unknowns ($\overline{u}_i$, $\overline{u_i u_j}$, $\overline{p}$) than equations. Hence, in order to advance the solution of the filtered quantities in time, a closure model for the nonlinear filtered advection term, $\overline{u_i u_j}$, needs to be provided, as well as the initial conditions for $\overline{u}_i$ and $\overline{p}$.

In a LES framework, Leonard's decomposition (Leonard 1974) separates $\overline{u_i u_j}$ into a large-scale part, $\overline{u}_i \overline{u}_j$, and a subfilter scale (SFS), or turbulent, stress tensor, τ_{ij}, i.e., $\overline{u_i u_j} = \overline{u}_i \overline{u}_j + \tau_{ij}$. Therefore, the conservation of filtered momentum can be recast in the form

$$\frac{\partial \overline{u}_i}{\partial t} + \frac{\partial (\overline{u}_i \overline{u}_j)}{\partial x_j} = -\frac{1}{\rho}\frac{\partial \overline{p}}{\partial x_i} + \nu \frac{\partial^2 \overline{u}_i}{\partial x_j \partial x_j} - \frac{\partial \tau_{ij}}{\partial x_j}. \tag{2.4}$$

The resolved scales of LES, $\overline{\phi}$, are characterized by the filter applied to the conservation equations. In a general context, the filtering and discretization operators are different (Lund 2003). However, in most cases the spatial discretization is chosen to be specifically the low-pass filter (Rogallo & Moin 1984), i.e., implicit filtering. Hence, τ_{ij} is habitually referred to as the subgrid-scale (SGS) tensor.

2.1. *Subgrid-scale models*

The objective of SGS models is to replace the unknown value of τ_{ij} by an approximate representation; τ_{ij}^{sgs} will be used throughout the paper to refer to the modeled τ_{ij}. In this regard, the eddy-viscosity assumption (Rogallo & Moin 1984) is the most widely used approach due to its robustness and dissipative character. This group of models represents

the anisotropic part of τ_{ij} as

$$\tau_{ij}^{sgs} - \frac{\tau_{kk}^{sgs}}{3}\delta_{ij} = -2\nu_{sgs}\overline{S}_{ij}, \tag{2.5}$$

where $\tau_{kk} = \tau_{11} + \tau_{22} + \tau_{33}$ is the trace of the tensor, ν_{sgs} is the turbulent viscosity predicted by the specific model (Smagorinsky 1963; Germano *et al.* 1991; Nicoud & Ducros 1999), and $\overline{S}_{ij} = 1/2(\partial\overline{u}_i/\partial x_j + \partial\overline{u}_j/\partial x_i)$ is the strain rate tensor of the resolved scales. In the LES of incompressible flows, the isotropic part, $\tau_{kk}/3$, is usually added to the filtered pressure, resulting in a modified pressure that the LES solution evolves in time. In the case of compressible flows, explicit subgrid models have been proposed for τ_{kk}^{sgs} (for example, see Yoshizawa (1986), Moin *et al.* (1991)).

3. Nonlinear filtered advection term

3.1. *Realizability conditions*

In the RANS approach, the ensemble average process confines all the turbulent effects in the Reynolds stresses, $R_{ij} = \overline{u'_i u'_j}$; here, u'_i and u'_j refer to the fluctuating components and $\overline{u'_i u'_j}$ is the averaged quantity of their product. Since the averaging operator is a statistical mean, in RANS modeling R_{ij} must be symmetric and positive semi-definite in order to ensure physically plausible values, i.e., non-negative real energies. This requirement is equivalent to the conditions of realizability (Schumann 1977) given by the following inequalities

$$R_{\alpha\alpha} \geq 0 \quad \text{for} \quad \alpha \in \{1,2,3\}, \tag{3.1}$$

$$R_{\alpha\beta}^2 \leq R_{\alpha\alpha}R_{\beta\beta} \quad \text{for} \quad \alpha \neq \beta, \tag{3.2}$$

$$\det(R_{ij}) \geq 0, \tag{3.3}$$

which guarantee that the spectrum of R_{ij} is non-negative and real. The summation convention is adopted for Latin, but not for Greek indices.

In a LES context, the common premise is that realizability conditions apply to τ_{ij}. However, rather than a physical requirement, this assumption is a modeling choice to restrict the closure space to non-negative real τ_{kk}^{sgs}. In fact, it has been demonstrated (Vreman *et al.* 1994) that the conditions are not satisfied for τ_{ij} if nonpositive filters are used. The most general requirement is that the divergence of the filtered advection term is real, i.e., $\partial(\overline{u_i u_j})/\partial x_j \in \mathbb{R}^3$. Nonetheless, the set of solutions satisfying this constraint is too large, and therefore impracticable from a modeling perspective. As a consequence, the approach chosen in this work is to impose realizability conditions to $\overline{u_i u_j}$, which is a compromise between generality and feasibility. In this regard, the conditions of realizability applied to $\overline{u_i u_j}$ read

$$\overline{u_\alpha u_\alpha} \geq 0 \quad \text{for} \quad \alpha \in \{1,2,3\}, \tag{3.4}$$

$$\overline{u_\alpha u_\beta}^2 \leq \overline{u_\alpha u_\alpha}\,\overline{u_\beta u_\beta} \quad \text{for} \quad \alpha \neq \beta, \tag{3.5}$$

$$\det(\overline{u_i u_j}) \geq 0. \tag{3.6}$$

3.2. *Tensor decomposition*

The nonlinear filtered advection term can be decomposed into factors by introducing the normalized anisotropy tensor, $\overline{a}_{ij}$, as

$$\overline{a}_{ij} = \frac{\overline{u_i u_j}}{\overline{u_k u_k}} - \frac{1}{3}\delta_{ij} = \overline{v}_{in}\overline{\Lambda}_{nl}\overline{v}_{jl}, \tag{3.7}$$

which is symmetric and trace-free, i.e., the eigenvalues sum zero. Moreover, its eigendecomposition is given by a matrix of orthonormal eigenvectors, $\overline{v}_{in}$, and a diagonal matrix of eigenvalues, $\overline{\Lambda}$, ordered such that $\overline{\lambda}_1 \geq \overline{\lambda}_2 \geq \overline{\lambda}_3$.

The realizability constraints, Eqs. 3.4-3.6, bound the intervals of the anisotropy tensor components. The diagonal elements, $\overline{a}_{\alpha\alpha}$, take minimum and maximum values if $\overline{u_\alpha u_\alpha} = 0$ and $\overline{u_\alpha u_\alpha} = \overline{u_k u_k}$, respectively, while, due to the positive semi-definiteness of $\overline{u_i u_j}$, the off-diagonal components, $\overline{a}_{\alpha\beta}$, reach their minimum and maximum values when $\overline{u_\alpha u_\beta} = \pm\overline{u_k u_k}$. Introducing these conditions in Eq. 3.7 results in the following intervals

$$-1/3 \leq \overline{a}_{\alpha\alpha} \leq 2/3 \quad \text{for} \quad \alpha \in \{1,2,3\}, \tag{3.8}$$

$$-1/2 \leq \overline{a}_{\alpha\beta} \leq 1/2 \quad \text{for} \quad \alpha \neq \beta. \tag{3.9}$$

Finally, the anisotropy tensor allows reformulating $\overline{u_i u_j}$ in terms of magnitude, $\overline{u_k u_k}$, shape, $\overline{\Lambda}_{nl}$, and orientation, $\overline{v}_{in}$, in the form

$$\overline{u_i u_j} = \overline{u_k u_k}\left(\overline{v}_{in}\overline{\Lambda}_{nl}\overline{v}_{jl} + \frac{1}{3}\delta_{ij}\right). \tag{3.10}$$

3.3. *The barycentric map*

For any anisotropy tensor, the diagonal matrix of eigenvalues characterizes the shape of a corresponding ellipsoid. Its major, medium and minor axes compose the basis of eigenvectors, with scalings equal to the values of the associated eigenvalues. The number of non-zero values, i.e., the rank, holds a direct connection to the limiting states of componentiality. In this work, componentiality primarily indicates the number of proper vectors of $\overline{u_i u_j}$ with non-zero scaling, but it can also be utilized to reflect the number of non-zero eigenvalues in the main directions of its resolved, $\overline{u}_i\overline{u}_j$, and modeled parts, τ_{ij}^{sgs}, or in the principal axes of the Reynolds stresses, R_{ij}.

Three limiting shapes exist in the case of a positive semi-definite second-order tensor. The one-component limiting state (rod-like) corresponds to a one-rank tensor where $2/3 = \lambda_1 > \lambda_2 = \lambda_3 = -1/3$. Similarly, the two-component axisymmetric limiting state (disk-like) presents two principal directions with equal non-zero eigenvalues of value $1/6 = \lambda_1 = \lambda_2 < \lambda_3 = -1/3$. Finally, the three-component isotropic limiting state (spherical) is characterized by a basis of eigenvectors with all eigenvalues equal to zero, i.e., $\lambda_1 = \lambda_2 = \lambda_3 = 0$.

Tensor anisotropy, or shape, is usually visualized by means of anisotropy-invariant maps (AIM). In the context of turbulence analysis, commom AIMs are the nonlinear Lumley (Lumley & Newman 1977) and turbulence (Choi & Lumley 2001) triangles or the linear eigenvalue map (Lumley & Newman 1977). An alternative construction is the barycentric map (Banerjee *et al.* 2007). This approach relies on the fact that any anisotropy state is a convex combination of the limiting states of componentiality. In an Euclidean space, these can be represented as the vertices of an equilateral triangle with coordinates $\mathbf{x}_{1c} = (0,0)$, $\mathbf{x}_{2c} = (1,0)$, and $\mathbf{x}_{3c} = (1/2, \sqrt{3}/2)$. A graphical representation of the map and the different anisotropy shapes is illustrated in Figure 1. One of the main advantages is its capacity to provide a linear relation between anisotropy eigenvalues and Euclidean space through the projection

$$\mathbf{x} = \mathbf{x}_{1c}\left(\lambda_1 - \lambda_2\right) + 2\mathbf{x}_{2c}\left(\lambda_2 - \lambda_3\right) + \mathbf{x}_{3c}\left(3\lambda_3 + 1\right). \tag{3.11}$$

This projection, together with the requirement that the eigenvalues sum zero, is a unique invertible linear mapping that can be mathematically expressed as $\mathbf{x} = \mathbf{B}\lambda_l$. Note that

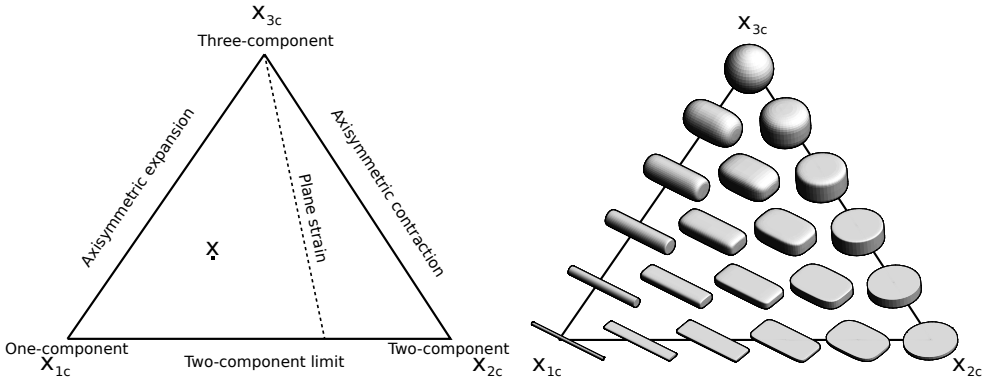

FIGURE 1. Barycentric map based on the eigenvalues of a general second-order anisotropy tensor. Left: limiting states of componentiality. Right: tensor shapes visualized with superquadric glyphs (Kindlmann 2004); figure regenerated using open-source software (Teem 2003).

realizability conditions imply that any anisotropy state of $\overline{u_i u_j}$, i.e., $\overline{\mathbf{x}}$, lies within the triangle.

4. Epistemic uncertainty estimation framework

The strategy to analyze model-form error in the underlying SGS closure is to introduce controlled perturbations into the nonlinear filtered advection term such that their impact on the QoI can be assessed. In a LES context, large scales are directly resolved, whereas model assumptions are confined to the subgrid scales. Consequently, in order to restrict the injection to τ_{ij}^{sgs}, the decomposed $\overline{u_i u_j}$ (Eq. 3.10) needs to be separated into resolved and modeled parts. This is accomplished through the following expression

$$\overline{u_i u_j} = \overline{u_k u_k}\left(a_{ij}^{res} + a_{ij}^{sgs} + \frac{1}{3}\delta_{ij}\right), \tag{4.1}$$

where a_{ij}^{res} and a_{ij}^{sgs} are the resolved and SGS components of the total anisotropy tensor given by

$$a_{ij}^{res} = \frac{1}{\overline{u_k u_k}}\left(\overline{u}_i\overline{u}_j - \frac{\overline{u}_k\overline{u}_k}{3}\delta_{ij}\right) = v_{in}^{res}\Lambda_{nl}^{res}v_{jl}^{res}, \tag{4.2}$$

$$a_{ij}^{sgs} = \frac{1}{\overline{u_k u_k}}\left(\tau_{ij}^{sgs} - \frac{\tau_{kk}^{sgs}}{3}\delta_{ij}\right) = v_{in}^{sgs}\Lambda_{nl}^{sgs}v_{jl}^{sgs}, \tag{4.3}$$

with $\overline{u}_k\overline{u}_k$ the resolved part of $\overline{u_k u_k}$.

Once the separation between resolved and modeled parts is performed, perturbations are defined as

$$\overline{u_i u_j}^* = \overline{u}_i\overline{u}_j + \tau_{ij}^{sgs*} = \overline{u}_i\overline{u}_j + \overline{u_k u_k}^* a_{ij}^{sgs*} + \frac{\tau_{kk}^{sgs*}}{3}\delta_{ij}, \tag{4.4}$$

$$\text{with} \quad \overline{u_k u_k}^* = \overline{u}_k\overline{u}_k + \tau_{kk}^{sgs*} \quad \text{and} \quad a_{ij}^{sgs*} = v_{in}^{sgs*}\Lambda_{nl}^{sgs*}v_{jl}^{sgs*}. \tag{4.5}$$

Thus, perturbations (indicated with *) are applied to the subgrid-scales only, and are specified as a discrepancy of the SGS tensor in terms of magnitude ($\tau_{kk}^{sgs*} = \tau_{kk}^{sgs} + \Delta\tau_{kk}^{sgs}$), shape (diagonal matrix Λ_{nl}^{sgs*} of perturbed eigenvalues λ_l^*), and orientation ($v_{ij}^{sgs*} = q_{in}v_{nj}^{sgs}$ with q_{in} an orthonormal rotation matrix).

4.1. *Modeled subgrid-scale tensor magnitude perturbation*

Lower and upper bounds for the perturbation of τ_{kk}^{sgs} can be obtained by considering the sign nature of the quantities composing the trace of the nonlinear filtered advection term. Its mathematical expression is

$$\overline{u_k u_k} = \overline{u}_k \overline{u}_k + \tau_{kk}^{sgs}, \tag{4.6}$$

where $\overline{u_k u_k}$ and $\overline{u}_k \overline{u}_k$ are non-negative. The former, $\overline{u_k u_k}$, is non-negative due to the restriction made in this work that realizability conditions apply to $\overline{u_i u_j}$, whereas the latter, $\overline{u}_k \overline{u}_k$, is non-negative by construction independently of the filter utilized, given its square product expression. In order to respect these properties, any possible perturbation of τ_{kk}^{sgs} is bounded by $\overline{u_k u_k} = \overline{u}_k \overline{u}_k + \tau_{kk}^{sgs} \geq 0$ and $\overline{u}_k \overline{u}_k = \overline{u_k u_k} - \tau_{kk}^{sgs} \geq 0$. Therefore, the intervals of magnitude discrepancy written in terms of $\Delta\tau_{kk}^{sgs}$ result in

$$-\overline{u}_k \overline{u}_k - \tau_{kk}^{sgs} \leq \Delta\tau_{kk}^{sgs} \leq \overline{u_k u_k} - \tau_{kk}^{sgs}. \tag{4.7}$$

Notice that expressions for $\overline{u_k u_k}$ and τ_{kk}^{sgs} are not typically considered in LES calculations. The latter is absorbed in the pressure term for incompressible flow, while commonly considered small for low-Mach-number and compressible flows. However, closures for its evaluation exist in the literature (for instance, the models proposed by Yoshizawa (1986) and Moin *et al.* (1991)). On the other hand, $\overline{u_k u_k}$ is always decomposed into resolved and modeled parts and, consequently, is never explicitly computed. Even so, deconvolution methods (Stolz & Adams 1999) are frequently utilized to approximate the subfilter velocity, ${u_i}'$, of the Navier-Stokes equations. To a first approximation, similar approaches could be applied to directly model $\overline{u_k u_k}$.

4.2. *Modeled subgrid-scale tensor eigenvalue perturbation*

Different strategies can be designed to perturb the eigenvalues of a_{ij}^{sgs}. Nonetheless, the framework proposed allows the perturbations to be defined implicitly through the coordinates in the barycentric map as $\lambda_l^{sgs*} = \mathbf{B}^{-1}\mathbf{x}^{sgs*}$ independently of their nature. For this initial study, we choose the uncertainty to be characterized by a direction, $\mathbf{x}^t - \mathbf{x}^{sgs}$, and a magnitude, $|\mathbf{x}^t - \mathbf{x}^{sgs}|$, both of which could vary in space and time. In particular, perturbations within the barycentric map are considered toward each of the three corners of the triangle, i.e., $\mathbf{x}_{1c}$, $\mathbf{x}_{2c}$, and $\mathbf{x}_{3c}$, and are defined by means of a relative distance Δ_B toward the target vertex. In mathematical form, the eigenvalue perturbation can be expressed through the following translation

$$\mathbf{x}^{sgs*} = \mathbf{x}^{sgs} + \Delta_B \left(\mathbf{x}^t - \mathbf{x}^{sgs}\right), \tag{4.8}$$

where $\mathbf{x}^{sgs}$, $\mathbf{x}^{sgs*}$, and $\mathbf{x}^t$ are the coordinates of the base-model prediction, new pertubed position and target corner, respectively. This process is illustrated in Section 4.2.1. Finally, by applying the linear map $\mathbf{B}$ to the new position $\mathbf{x}^{sgs*}$, the perturbed eigenvalues are uniquely defined as

$$\lambda_l^{sgs*} = (1 - \Delta_B)\,\lambda_l^{sgs} + \Delta_B \lambda_l^t. \tag{4.9}$$

4.2.1. *Graphical representation*

Injection of uncertainty into the modeled part of $\overline{u_i u_j}$ is represented in Figure 2. First, the eigenvalues of the resolved and SGS base-model tensors determine the initial location of $\overline{a}_{ij}$ in the map, $\overline{\mathbf{x}}$. Note that $\overline{\mathbf{x}}$ is not a direct summation of $\mathbf{x}^{res}$ and $\mathbf{x}^{sgs}$ since the eigenvectors of the tensors are, in general, different. In particular, this example depicts the case in which the shape of a_{ij}^{res} is predominantly rod-like, and the SGS tensor is

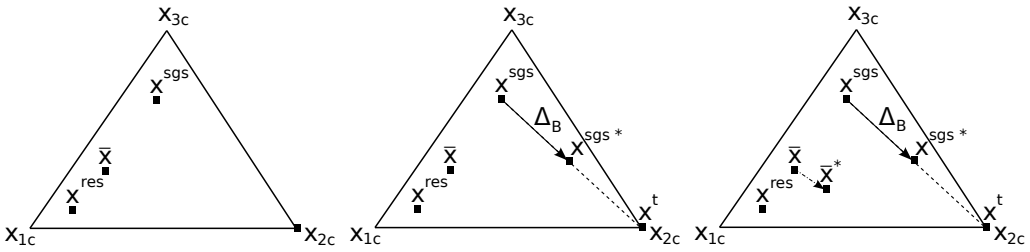

FIGURE 2. Sequential illustration of the eigenvalue perturbation procedure. The resolved, $\mathbf{x}^{res}$, and SGS base-model, $\mathbf{x}^{sgs}$, parts provide an initial location $\overline{\mathbf{x}}$ within the triangle (left). A perturbation of magnitude Δ_B toward $\mathbf{x}_{2c}$ is applied to $\mathbf{x}^{sgs}$ (center). The new location of the SGS part, $\mathbf{x}^{sgs*}$, indirectly modifies the coordinates of $\overline{\mathbf{x}}$, resulting in a perturbed state $\overline{\mathbf{x}}^*$ (right).

approximated by an eddy-viscosity-type model. Subsequently, uncertainty is introduced by applying a translation to $\mathbf{x}^{sgs}$ of magnitude Δ_B toward $\mathbf{x}^t$ ($\mathbf{x}_{2c}$ in this example), resulting in the perturbed location $\mathbf{x}^{sgs*}$. Finally, the perturbation to the eigenvalues of the SGS part, together with the contribution from the resolved scales, induces a new location within the barycentric map indicated as $\overline{\mathbf{x}}^*$.

4.3. *Modeled subgrid-scale tensor eigenvector perturbation*

The methodology to introduce perturbations into the eigenvectors of a_{ij}^{sgs} is based on the physical constraints of energy transfer between resolved and modeled scales. The starting point is the balance equation for resolved filtered kinetic energy, $E_f = \overline{u}_k\overline{u}_k/2$, given as (Pope 2000)

$$\frac{\partial E_f}{\partial t} + \overline{u}_j\frac{\partial E_f}{\partial x_j} - \frac{\partial}{\partial x_i}\left[\overline{u}_j\left(2\nu\overline{S}_{ij} - \tau_{ij} - \frac{1}{\rho}\overline{p}\,\delta_{ij}\right)\right] = -\epsilon_f - \mathcal{P}_r. \tag{4.10}$$

The terms on the left-hand side represent transport, while the terms on the right-hand side correspond to viscous dissipation, $\epsilon_f = 2\nu\overline{S}_{ij}\overline{S}_{ij}$, and rate of production of SGS kinetic energy, $\mathcal{P}_r = -\tau_{ij}\overline{S}_{ij}$. The latter is of particular interest since it represents the transfer of energy between resolved and modeled scales. On average, $\mathcal{P}_r$ typically transfers energy from large to small scales, i.e., forward-scatter. However, it can present positive or negative values instantaneously, and therefore, it can act as a sink (forward-scatter) or source (backscatter) term for E_f (Piomelli *et al.* 1991).

In the above equation, the transport of SGS stresses, $\partial(\overline{u}_j\tau_{ij})/\partial x_i$, and $\mathcal{P}_r$ require closure through τ_{ij}. However, modeling $\partial(\overline{u}_j\tau_{ij})/\partial x_i$ involves non-local information due to the differentiation operator. From the applicability viewpoint, this requirement complicates its utilization as a constraint on the perturbations in the eigenvector basis. By contrast, $\mathcal{P}_r$ is purely local since it only involves single-point matrix operations. In addition, its direct connection with the transfer of energy between resolved and modeled scales provides physical meaning to the injection of uncertainty.

The SGS kinetic energy production rate term is an inner product between τ_{ij} and $\overline{S}_{ij}$, which is equivalent to $\mathcal{P}_r = \mathrm{tr}(-\tau_{ij}\overline{S}_{ij})$. In this regard, the value of the inner product depends on the alignment between the eigenvectors of τ_{ij} and $\overline{S}_{ij}$. Diverse alignments between these two tensors can be considered. However, for the purpose of enveloping the possible dynamics, the methodology proposed seeks the extremal values of this inner product. In the case of τ_{ij} being real and $\overline{S}_{ij}$ real symmetric, the lower and upper bounds are given by the following expression (Lasserre 1995)

$$\lambda_1\gamma_3 + \lambda_2\gamma_2 + \lambda_3\gamma_1 \leq \mathcal{P}_r \leq \lambda_1\gamma_1 + \lambda_2\gamma_2 + \lambda_3\gamma_3, \tag{4.11}$$

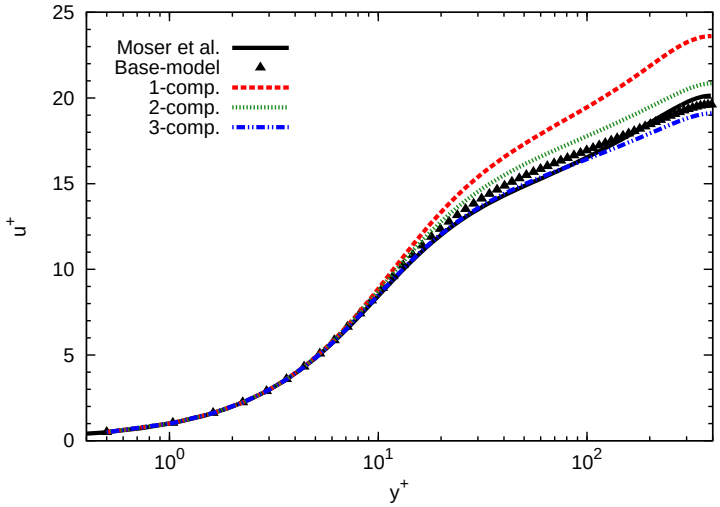

FIGURE 3. Effect of SGS stress tensor eigenvalue perturbation on mean streamwise velocity profile (quantities in wall units). DNS data from Moser *et al.* (1999) (solid line), base-model solution (solid triangles), eigenvalue perturbation results (dashed lines).

with λ_l and γ_l the eigenvalues of τ_{ij} and $\overline{S}_{ij}$, respectively. The upper bound in this inequality corresponds to the situation in which τ_{ij} and $\overline{S}_{ij}$ share the same basis of eigenvectors, while the lower bound is the case in which the eigenvector bases are the same except for a permutation between the first and third eigenvectors. From a practical point of view, the existence of bounds suggests that only two eigenvector sets need to be considered. These can be easily analyzed by setting the perturbed eigenvectors of τ_{ij}^{sgs} to be the eigenvectors of $\overline{S}_{ij}$ with and without a permutation of its first and third eigenvectors.

Caution is required, however, when considering the case with permuted eigenvectors. Its negative character introduces backscatter into the discrete system and may result in finite time blow-up of the kinetic energy. In this regard, if perturbations vary in time and space, the only requirement necessary is to satisfy the second law of thermodynamics, i.e., the net transport of energy is of forward-scatter type. On the contrary, if perturbations are constant in space and time, one possible local constraint is to impose the perturbed SGS kinetic energy production rate term to be smaller in magnitude than the viscous dissipation, i.e., $|\mathrm{tr}(-\tau_{ij}^{sgs*}\overline{S}_{ij})| \leq 2\nu\mathrm{tr}(\overline{S}_{ij}^2)$.

5. Numerical experiments

The performance of the epistemic UQ framework proposed is investigated by computing LES of turbulent flow with the unstructured and massively parallel Nalu open-source code (Domino 2015). In this exploratory work, only constant homogeneous perturbations to the anisotropy and orientation of the modeled SGS tensor are considered. Incertitude in the magnitude of τ_{ij}^{sgs}, as well as spatio-temporal varying perturbations, are being investigated and will be discussed in future works. In this section, results corresponding to the WALE model (Nicoud & Ducros 1999) without perturbations are referred to as base-model solutions, while computations where shape or orientation uncertainty has

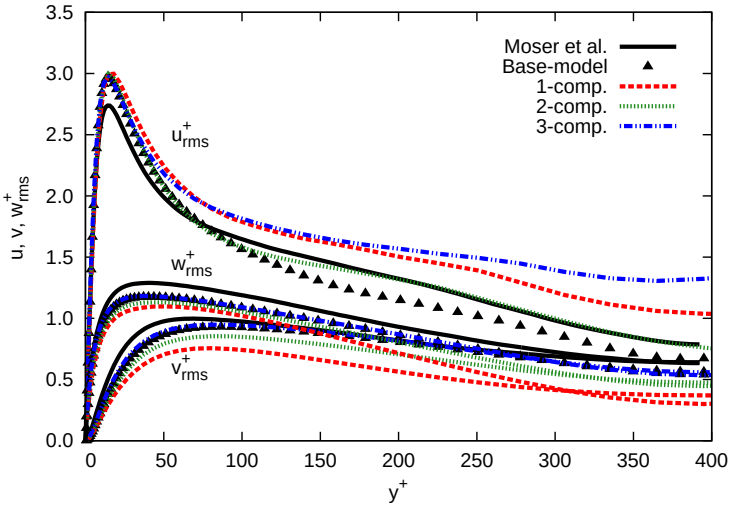

FIGURE 4. Effect of SGS stress tensor eigenvalue perturbation on rms velocity fluctuations (quantities in wall units). DNS data from Moser *et al.* (1999) (solid line), base-model solution (solid triangles), eigenvalue perturbation results (dashed lines).

been introduced are designated by the target corner (1-comp., 2-comp., or 3-comp.) or eigenvector permutation (perm. 1, perm. 2, or perm. 3) of the respective perturbation.

5.1. *Turbulent channel flow*

The canonical periodic channel flow at friction Reynolds number $Re_\tau = 395$ is selected as test case; numerical results will be compared to reference DNS data by Moser *et al.* (1999). As is customary, $Re_\tau = u_\tau h/\nu$, with u_τ being the friction velocity, h the channel half-height, and ν the molecular kinematic velocity of the fluid. The mass flow rate is determined through a static pressure gradient $dp/dx = -\tau_w/h$, where τ_w is the wall shear stress. The computational domain is $2\pi h \times 2h \times \pi h$ in the streamwise (x), vertical (y), and spanwise (z) directions, respectively. Streamwise and spanwise boundaries are set periodic, and no-slip conditions are imposed to the vertical boundaries. The grid is uniform in the streamwise and spanwise directions with spacings in wall units equal to $\Delta x^+ = 38.8$ and $\Delta z^+ = 12.9$, while stretched in the vertical direction with the first grid point at $y^+ = 0.5$ and with spacings in the range $\Delta y^+ = [0.5 - 15.1]$. This grid arrangement corresponds to a wall-resolved LES of size $64\times128\times96$. The simulations start from a sinusoidal velocity field from which turbulence develops after several time units. For each calculation, the averaging process is started once a sufficiently long transient period is surpassed to ensure independence from the initial condition.

5.2. *Uncertainty in tensor anisotropy*

Epistemic uncertainty in the spectrum of τ_{ij}^{sgs} is analyzed by perturbing the eigenvalues of the base-model tensor. Three cases are considered in which the anisotropy of the SGS tensor is forced toward the limiting states of the barycentric map. As described in Section 4.2, these cases correspond to perturbations toward the one-component (1-comp.), two-component (2-comp.), and three-component (3-comp.) vertices of the triangle with relative distances, Δ_B, of value 0.001, 0.001, and 1.0, respectively. The order of magnitude difference between 1- or 2- and 3-comp. perturbations is due to the initial base-model tensor state. The WALE model belongs to the eddy-viscosity-type family, and therefore its

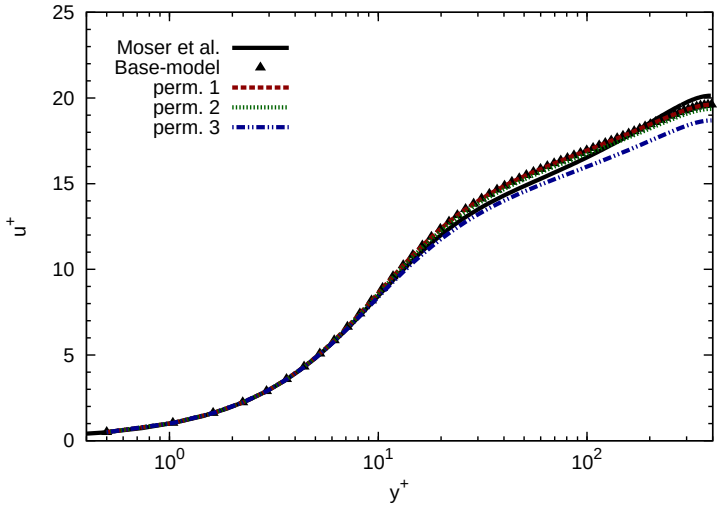

FIGURE 5. Effect of SGS stress tensor eigenvector perturbation on mean streamwise velocity profile (quantities in wall units). DNS data from Moser *et al.* (1999) (solid line), base-model solution (solid triangles), eigenvector perturbation results (dashed lines).

spectrum is inherently constructed to be close to the three-component isotropic vertex of the $\overline{u_i u_j}$'s barycentric map. In this regard, 1- and 2-comp. perturbations are significantly small in relative distance, however, they are rather large in absolute value with respect to the 3-comp. perturbation. Moreover, the fact that perturbations are constant in time and uniform in space for a relatively low-Reynolds-number case, forces perturbations to remain small in order to ensure that realistic flow configurations are obtained.

The QoI considered to analyze the effects of the perturbations is the mean streamwise velocity profile (Figure 3), which is compared to DNS and base-model results. Rather than accurately predicting the solution of turbulent flow, the objective of the UQ epistemic framework is to provide bounds for the QoI; detailed solution of the flow is not known in engineering applications and, consequently, the aim of computational studies is to produce solution bounds useful for design or optimization processes. For example, Figure 3 shows that perturbations to the anisotropy of τ_{ij}^{sgs} results in a bounding interval for the mean streamwise velocity profile. In particular at $y^+ = Re_\tau$, the solution interval is limited by the 1- and 3-comp. perturbations with values $u^+ = 23.6$ and 19.1, respectively, and which satisfactorily envelope the base-model prediction ($u^+ = 19.6$) and DNS result ($u^+ = 20.1$).

The outcome of eigenvalue perturbation is better comprehended by considering the average profiles of rms velocity fluctuations plotted in Figure 4. In comparison to the base-model solution, forcing τ_{ij}^{sgs} to be more rod-like reduces the rms velocity fluctuations in the vertical and spanwise directions of the flow. This reduction results in an overall laminarization of the flow and, consequently, the mass flow rate for a given static pressure gradient is increased. By contrast, perturbations toward the isotropic limiting state enhances fluctuations, resulting in a flow regime with levels of turbulence higher than in the base-model prediction. These two behaviors are captured by the mean velocity profile as larger and smaller values of mass flow rate are obtained, respectively.

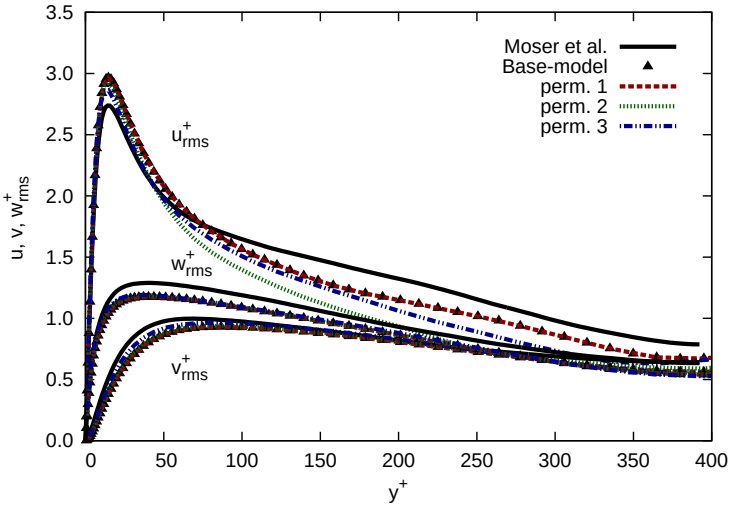

FIGURE 6. Effect of SGS stress tensor eigenvector perturbation on rms velocity fluctuations (quantities in wall units). DNS data from Moser *et al.* (1999) (solid line), base-model solution (solid triangles), eigenvalue perturbation results (dashed lines).

5.3. *Uncertainty in tensor orientation*

Propagation of incertitude in the orientation of the modeled SGS stress tensor is studied by constructing τ_{ij}^{sgs} based on rearrangements of the eigenvectors of $\overline{S}_{ij}$. As discussed in Section 4.3, two limiting states of eigenvector perturbation should be sufficient. However, three cases are considered for completeness. The first permutation (perm. 1) sets the eigenvectors of τ_{ij}^{sgs} directly equal to the proper basis of $\overline{S}_{ij}$. The third permutation is exactly equal to perm. 1, but with a shift between the first and third eigenvectors. Finally, the second permutation (perm. 2) is an intermediate case in which the second and third eigenvectors of perm. 1 are interchanged. No additional modifications are required except for perm. 3 in which, due to the sustained introduction of kinetic energy from the SGS to the resolved scales (backscatter), a constraint is imposed on the magnitude of τ_{ij}^{sgs} to ensure that viscous forces are able to locally dissipate sufficient SGS kinetic energy.

Variations in the QoI due to the three eigenvector perturbations are plotted in Figure 5 together with the base-model and DNS solutions. The first observation is that the two limiting candidates proposed for enveloping the uncertainty in eigenvector basis are successful, i.e., the result of perm. 2 is bounded by the solutions of perm. 1 and perm. 3. The second observation is that perm. 1 and base-model give the same solution. This result can be readily explained by noticing that eddy-viscosity-type models are basically constructed from single-point multiplications of $\overline{S}_{ij}$ and scalars values of the form $-2\nu_{sgs}$. Therefore, solutions from eddy-viscosity models directly provide one of the uncertainty bounds in SGS stress tensor orientation.

The physical mechanism responsible for the change in mean streamwise velocity profile is inferred from the rms velocity fluctuations depicted in Figure 6. In the case of perm. 1, the orientation of the SGS stress tensor is exactly equal to the eigenvector basis of $\overline{S}_{ij}$. This alignment between tensors forces the inner product $\mathcal{P}_r$ to be defined positive. As a result, the SGS kinetic energy production rate term in Eq. 4.10 acts as a sink extracting energy from the resolved to the modeled scales and, consequently, reduces the magnitude of the velocity fluctuations. At the opposite extreme, perm. 3 continuously energizes the

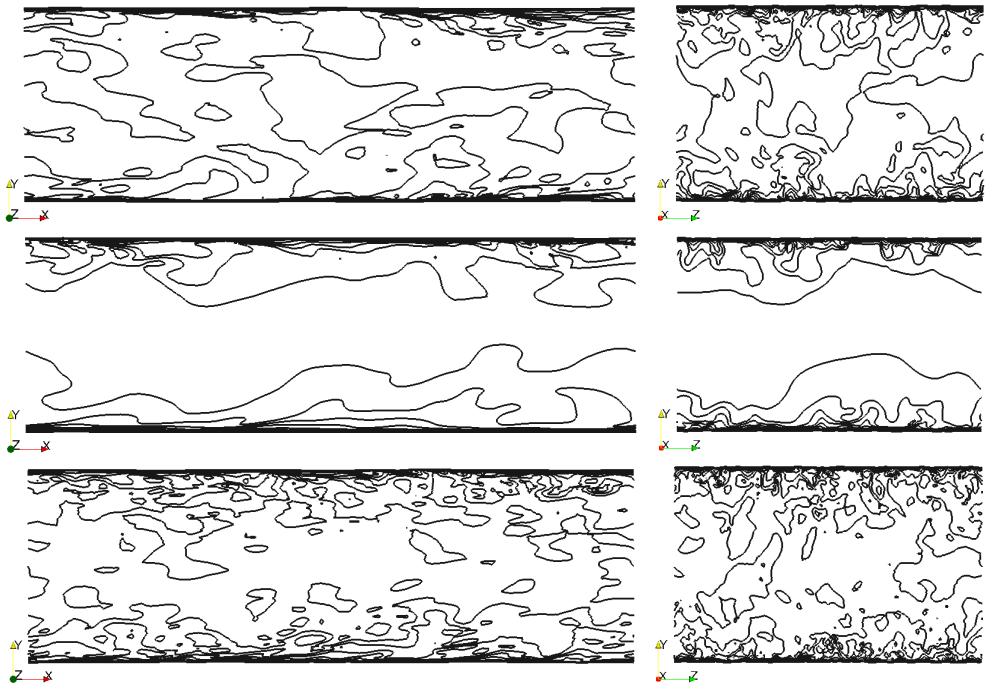

FIGURE 7. Effect of SGS stress tensor perturbation on instantaneous streamwise velocity (contours). Base-model (top), 1-comp. eigenvalue perturbation (center), perm. 3 eigenvector perturbation (bottom). Images correspond to the xy- (left) and yz-plane (right) views.

flow by setting $\mathcal{P}_r$ to be negative, thereby acting as a source of kinetic energy from the small to the large scales. Different magnitude levels in the effects of perm. 3 can be obtained by modifying the constraint required to guarantee that the second law of thermodynamics is satisfied in an average sense. Nonetheless, we find the local condition proposed in this work to be highly effective from a computational perspective.

5.4. *Qualitative comparison of instantaneous flow field*

To further illustrate the effects of the perturbations, contours of instantaneous streamwise velocity for the 1-comp. and perm. 3 cases are visually compared to the base-model solution in Figure 7. Taking as a reference the base-model velocity field (top row), perturbing toward the one-component limiting state (center row) results in a reduction in turbulence intensity levels, especially at the centerline region of the channel where the SGS model is active; the WALE model recovers cubic behavior in the vicinity of solid boundaries. Conversely, perturbation of the SGS stress tensor orientation by means of perm. 3 (bottom row) has a net effect of increasing the magnitude of the velocity fluctuations. In comparison to the base-model prediction, this increase results in more fragmented flow structures which are indicative of solutions presenting higher levels of turbulence.

6. Conclusions and future work

The aim of this work has been to develop a framework for estimating epistemic uncertainty in LES closures that goes beyond traditional non-intrusive sensitivity studies. The approach proposed is based on decomposing the SGS stress tensor such that incertitude

can be independently injected as discrepancy in magnitude (trace), anisotropy (eigenvalues), and orientation (eigenvectors) of the normalized turbulent stresses with respect to a particular tensor state. In addition, physically reasonable bounds for estimating uncertainty are proposed for each of the six degrees of freedom of the methodology.

The performance of the UQ framework is tested by computing LES of wall-resolved turbulent channel flow, and comparing the solution of the perturbed cases to the results predicted by the WALE SGS model and DNS reference data. The numerical results focus on spatially uniform perturbations to the shape and orientation of the SGS stress tensor. The results demonstrate the capability of the strategy to provide bounds for the QoI that envelop the base-model prediction and DNS solution. This capability is of great importance for utilizing the proposed UQ estimation approach in computational studies involving engineering applications. Furthermore, the advantage of decomposing the tensor in magnitude, shape and orientation is illustrated by giving direct physical interpretation of the effects of the perturbations introduced.

Ongoing work is focused on analyzing the effects of introducing uncertainty in the magnitude of the turbulent stresses, as well as combinations of different perturbations. At the same time, exploratory studies are being performed to develop non-uniform perturbation strategies to restrict the injection of incertitude to regions of the flow where the models are expected to provide less accurate predictions. For example, regions of transverse (Prandtl's second kind of secondary flow) mean motion in turbulent square duct flow, thin separating shear layers in flows over circular cylinders, or reverse vorticity zones in flows over backward-facing steps.

Acknowledgments

This investigation was funded by the United States Department of Energy's (DoE) National Nuclear Security Administration (NNSA) under the Predictive Science Academic Alliance Program II (PSAAP II) at Stanford University.

REFERENCES

Banerjee, S., Krahl, R., Durst, F. & Zenger, C. 2007 Presentation of anisotropy properties of turbulence, invariants versus eigenvalues approaches. *J. Turbul.* **8**, 1–27.

Choi, K.-S. & Lumley, J. L. 2001 The return to isotropy of homogeneous turbulence. *J. Fluid Mech.* **436**, 59–84.

DoE 2012 Workshop on extreme-scale solvers: transition to future architectures. U.S. Department of Energy, Office of Advanced Scientific Computing Research.

Domino, S. P. 2015 Sierra Low Mach Module: Nalu Theory Manual 1.0. SAND2015-3107W, Sandia National Laboratories, Unclassified Unlimited Release (UUR), https://github.com/NaluCFD/NaluDoc.

Emory, M., Larsson, J. & Iaccarino, G. 2013 Modeling of structural uncertainties in Reynolds-averaged Navier-Stokes closures. *Phys. Fluids* **25**, 110822.

Germano, M., Piomelli, U., Moin, P. & Cabot, W. 1991 A dynamic subgrid-scale eddy viscosity model. *Phys. Fluids A* **3**, 1760–1765.

Gorlé, C. & Iaccarino, G. 2013 A framework for epistemic uncertainty quantification of turbulent scalar flux models for Reynolds-averaged Navier-Stokes simulations. *Phys. Fluids* **25**, 055105.

Kindlmann, G. 2004 Superquadric tensor glyphs. *Proc. Sixth Joint Eurographics-IEEE TCVG* pp. 147–154.

Lasserre, J. B. 1995 A trace inequality for matrix product. *IEEE Trans. Autom. Control* **40**, 1500–1501.

Leonard, A. 1974 Energy cascade in large-eddy simulations of turbulent fluid flows. *Adv. Geophys. A* **18**, 237–248.

Lucor, D., Meyers, J. & Sagaut, P. 2007 Sensitivity analysis of large-eddy simulations to subgrid-scale-model parametric uncertainty using polynomial chaos. *J. Fluid Mech.* **585**, 255–280.

Lumley, J. L. & Newman, G. 1977 The return to isotropy of homogeneous turbulence. *J. Fluid Mech.* **82**, 161–178.

Lund, T. S. 2003 The use of explicit filters in large eddy simulation. *Comput. Math. Appl.* **46**, 603–616.

Meldi, M., Lucor, D. & Sagaut, P. 2011 Is the Smagorinsky coefficient sensitive to uncertainty in the form of the energy spectrum? *Phys. Fluids* **23**, 125109.

Meyers, J. & Sagaut, P. 2007*a* Evaluation of Smagorinsky variants in large-eddy simualtions of wall-resolved plane channel flows. *Phys. Fluids* **19**, 095105.

Meyers, J. & Sagaut, P. 2007*b* Is plane-channel flow a friendly case for the testing of large-eddy simulation subgrid-scale models? *Phys. Fluids* **19**, 048105.

Moin, P., Squires, K., Cabot, W. & Lee, S. 1991 A dynamic subgrid-scale model for compressible turbulence and scalar transport. *Phys. Fluids* **3**, 2746–2757.

Moser, R. D., Kim, J. & Mansour, N. N. 1999 Direct numerical simulation of turbulent channel flow up to $Re_\tau = 590$. *Phys. Fluids* **11**, 943–945.

Nicoud, F. & Ducros, F. 1999 Subgrid-scale stress modelling based on the square of the velocity gradient. *Flow Turbul. Combust.* **62**, 183–200.

Piomelli, U., Cabot, W., Moin, P. & Lee, S. 1991 Subgrid-scale backscatter in turbulent and transitional flows. *Phys. Fluids* **3**, 1766–1771.

Pope, S. B. 2000 *Turbulent flows*. Cambridge University Press.

Rogallo, R. S. & Moin, P. 1984 Numerical simulation of turbulent flow. *Annu. Rev. Fluid Mech.* **16**, 99–137.

Schumann, U. 1977 Realizability of Reynolds-stress turbulence models. *Phys. Fluids* **20**, 721–725.

Smagorinsky, J. 1963 General circulation experiments with the primitive equations. I. The basic experiment. *Mon. Weather Rev.* **91**, 99–164.

Stolz, S. & Adams, A. 1999 An approximate deconvolution procedure for large-eddy simulation. *Phys. Fluids* **11**, 1699–1701.

Teem Project 2003 Teem: Tools to process and visualize scientific data and images. http://teem.sourceforge.net.

Vreman, B., Geurts, B. & Kuerten, H. 1994 Realizability conditions for the turbulent stress tensor in large-eddy simulation. *J. Fluid Mech.* **278**, 351–362.

Yoshizawa, A. 1986 Statistical theory for compressible turbulent shear flows, with the application to subgrid modeling. *Phys. Fluids* **29**, 2152–2164.